Improvements in cosmological constraints from breaking growth degeneracy

Louis Perenon, Stéphane Ilíc, Roy Maartens, Alvaro de La Cruz-Dombriz

A&A 642, A116 (2020)
https://doi.org/10.1051/0004-6361/202038409

Astronomy & Astrophysics

Improvements in cosmological constraints from breaking growth degeneracy

L. Perenon[1], S. Ilić[2], R. Maartens[1,3], and A. de la Cruz-Dombriz[4,5,6]

[1] Department of Physics and Astronomy, University of the Western Cape, Cape Town 7535, South Africa
e-mail: perenon.louis@yahoo.fr
[2] Université PSL, Observatoire de Paris, Sorbonne Université, CNRS, LERMA, 75014 Paris, France
[3] CEICO, Institute of Physics of the Czech Academy of Sciences, Na Slovance 2, Praha 8, Czech Republic
[4] IRAP, Université de Toulouse, CNRS, CNES, UPS, Toulouse, France
[5] Institute of Cosmology & Gravitation, University of Portsmouth, Portsmouth PO1 3FX, UK
[6] Cosmology & Gravity Group, Department of Mathematics & Applied Mathematics, University of Cape Town, Rondebosch 7701, Cape Town, South Africa

Received 13 May 2020 / Accepted 22 July 2020

ABSTRACT

Context. The key probes of the growth of a large-scale structure are its rate f and amplitude σ_8. Redshift space distortions in the galaxy power spectrum allow us to measure only the combination $f\sigma_8$, which can be used to constrain the standard cosmological model or alternatives. By using measurements of the galaxy-galaxy lensing cross-correlation spectrum or of the galaxy bispectrum, it is possible to break the $f\sigma_8$ degeneracy and obtain separate estimates of f and σ_8 from the same galaxy sample. Currently there are very few such separate measurements, but even this allows for improved constraints on cosmological models.
Aims. We explore how having a larger and more precise sample of such measurements in the future could constrain further cosmological models.
Methods. We considered what can be achieved by a future nominal sample that delivers an ∼1% constraint on f and σ_8 separately, compared to the case with a similar precision on the combination $f\sigma_8$.
Results. For the six cosmological parameters of ΛCDM, we find improvements of ∼5–50% on their constraints. For modified gravity models in the Horndeski class, the improvements on these standard parameters are ∼0–15%. However, the precision on the sum of neutrino masses improves by 65% and there is a significant increase in the precision on the background and perturbation Horndeski parameters.

Key words. dark energy – large-scale structure of Universe

1. Introduction

The growth of a large-scale structure is sensitive to the theory of gravity and its measurement is a powerful test of the standard and alternative models of cosmology. It is characterised at the most basic level by the rate of growth $f = -\mathrm{d}\ln D/\mathrm{d}\ln(1+z)$, where $D(z)$ is the growth function of the linear matter density contrast, $\delta(z,\boldsymbol{k}) = D(z)\delta(z_{\rm in},\boldsymbol{k})/D(z_{\rm in})$, given an initial redshift $z_{\rm in}$. This rate governs the evolution of peculiar velocities, whose impact on the observed galaxy power spectrum is to introduce a redshift space distortion (RSD). The measurement of this anisotropy at redshift z delivers an estimate of $f(z)\sigma_8(z)$, where σ_8 fixes the amplitude of the matter density fluctuations. The degeneracy between f and σ_8 echoes the degeneracy between the linear galaxy bias and σ_8, and it cannot be broken via RSD power spectrum measurements alone.

The degeneracy can be broken by using an alternative observable in the galaxy sample that involves σ_8 or f. For example, combining RSD power spectrum measurements with galaxy-galaxy lensing measurements has produced separate estimates of f and σ_8 (de la Torre et al. 2017; Shi et al. 2018; Jullo et al. 2019). There are currently only a handful of such estimates, but even with only three separated data pairs, constraints on cosmological models improve noticeably (Perenon et al. 2019). Another way to break the degeneracy is by combining RSD measurements in the power spectrum and bispectrum (Gil-Marín et al. 2017).

Breaking the growth degeneracy is expected to break degeneracies between certain cosmological and modified gravity parameters. Here we confirm this expectation by computing the improvement in precision when using future separated measurements of f and σ_8 as compared to using the usual combined measurements $f\sigma_8$. We make forecasts for the standard Λ cold dark matter (CDM) model and for scalar-tensor theories in the Horndeski class (Horndeski 1974), using the effective field theory (EFT) of dark energy (DE; Gubitosi et al. 2013; Bloomfield et al. 2013), see Frusciante & Perenon (2020) for a recent review and Gleyzes et al. (2016), Alonso et al. (2017), Leung & Huang (2017), Abazajian et al. (2016), Reischke et al. (2019), Spurio Mancini et al. (2018), Frusciante et al. (2019), Ballardini et al. (2019) for more general Horndeski forecasts).

2. Models

We consider two models to assess the constraining power of the different growth of structure quantities. The first is the standard cosmological model ΛCDM, whose free parameters are (Planck Collaboration V 2020)

$$\{\Omega_{\rm b}h^2, \Omega_{\rm c}h^2, H_0, \tau, A_{\rm s}, n_{\rm s}, \Sigma m_\nu\}, \tag{1}$$

where the total neutrino mass $\sum m_\nu$ is equally shared by the three degenerate species. For the second, we chose the popular benchmark for studies of alternative gravitational models (Frusciante & Perenon 2020) that are Horndeski theories (Horndeski 1974). They are the most general covariant scalar-tensor theories with direct second-order equations of motion. We use in particular their description of linear perturbations provided by the α-EFT basis Bellini & Sawicki (2014). Bellini & Sawicki (2014) provide complete details of the construction of the action.

Observations suggest that the speed of gravitational waves is equal to that of light (Abbott et al. 2017a,b). This reduces the number of redshift-dependent functions in the effective description that govern how modifications of gravity affect perturbations to three:

$\alpha_M(z)$ – evolution of the effective Planck mass;
$\alpha_B(z)$ – mixing between the metric and DE field;
$\alpha_K(z)$ – kinetic energy of scalar perturbations.

Although α_K has virtually no effect on constraints from current data (Bellini et al. 2016; Frusciante et al. 2019), it needs to be included as a free parameter, since it regulates the propagation speed of DE perturbations. Setting it arbitrarily to zero could restrict the space of stable models and thus bias the constraints (Kreisch & Komatsu 2018; Frusciante et al. 2019).

The functional forms of $\alpha_I(z)$, $I = M, B, K$, are not given by the effective description. For simplicity, we use the effective DE parametrisation (Piazza et al. 2014; Bellini & Sawicki 2014) common in the literature,

$$\alpha_I(z) = a_I \frac{\Omega_x(z)}{\Omega_{x,0}}. \tag{2}$$

We also allow for deviations from a ΛCDM background by using the Chevallier-Polarski-Linder (CPL; Chevallier & Polarski 2001; Linder 2003) parametrisation for the effective DE equation of state of the Horndeski models:

$$w_x(z) = w_0 + w_a \frac{z}{1+z}. \tag{3}$$

In summary, the Horndeki model we consider contains five additional free parameters with respect to ΛCDM:

$$\{\Omega_b h^2, \Omega_c h^2, H_0, \tau, A_s, n_s, \Sigma m_\nu, w_0, w_a, a_M, a_B, a_K\}. \tag{4}$$

The ΛCDM model is recovered for $w_0 = -1$ and $w_a = a_M = a_B = a_K = 0$.

3. Methodology

The cosmological evolution of the models was computed using the Boltzmann code[1] `CLASS` (Blas et al. 2011), and its modified version[2] `hi_class` (Zumalacarregui et al. 2017; Bellini et al. 2020). The cosmological data – hereafter referred to as the "baseline" – contain the SDSS-II/SNLS3 Joint Light-curve Analysis (JLA) sample of type Ia supernova (SNIa; Betoule et al. 2014), the Baryon Oscillation Spectroscopic Survey (BOSS) baryon acoustic oscillation (BAO) measurements (Beutler et al. 2011; Anderson et al. 2014; Ross et al. 2015), and the low- and high-multipole temperature and polarisation of Planck 2018 cosmic microwave background (CMB) data (Planck Collaboration V 2020). We chose not to include CMB lensing data to avoid inconsistencies related to potential ΛCDM-dependent assumptions made during the lensing reconstruction.

Our aim was to focus on the gain from breaking growth degeneracy, rather than making realistic mocks and forecasts. In order to compare the constraining power of separated measurements of f and σ_8 with the combined measurements $f\sigma_8$, we simulated data for a nominal future galaxy sample that delivered a one percent precision for f, σ_8, and $f\sigma_8$. We assumed a redshift range containing ten measurements at $z = 0.1, 0.2, \ldots, 1$. The effects of extending the redshift range are studied in Sect. 4.3. We anticipate that a Stage IV experiment conducting a spectroscopic galaxy count survey together with a weak lensing survey, such as Euclid (Amendola et al. 2018), should be able to achieve close to 1% precision on $f\sigma_8$, f, and σ_8, using Planck priors on standard cosmological parameters.

Whenever needed, the growth quantities are computed with `CLASS` or `hi_class`. In order to compare the constraints on the same footing and avoid non-linear model dependencies, we computed the growth quantities with the linear power spectrum only. The values of σ_8 were obtained via the usual weighted integral of the linear power spectrum and f was computed as the log derivative $f = -(1+z)\mathrm{d}\ln\sigma_8/\mathrm{d}\ln z$ for simplicity.

As fiducial parameters we used the best-fit values obtained from the baseline constraints for the ΛCDM and Horndeski models. Then we created three sets of mocks for both models (for f, σ_8, and $f\sigma_8$), each exactly centred on their fiducial, meaning no random variance added to the data. The ΛCDM model has been shown to lie in a corner of the parameter space of stable Horndeski models (Piazza et al. 2014), which are ghost- and gradient-free models. When performing forecasts using Markov chain Monte Carlo (MCMC) methods, the stability priors can lead to a disfavouring of models lying close to the corner, purely due to volume effects and independently of their actual likelihood. Such considerations may have a significant effect on our results. This is hinted at for example by the highly irregular posteriors in the baseline case in Fig. 3 (grey contours) and the mismatch between their maximum and the best-fit model (dotted lines), characteristic of non-negligible prior effects. We can however expect those effects to be mitigated when additional data is added to the analysis, due to the fact that our Horndeski fiducial model (derived from the baseline best fit and used to produce our mocks) lies noticeably away from the "ΛCDM corner". Even if our MCMC explorations were impacted by such priors, this should not affect our conclusions since we always make statements regarding relative improvements.

4. Constraints

The sampling of all the considered likelihoods, as well as the computation of best-fit parameters, are performed using the publicly available[3] suite of codes ECLAIR (Ilić et al. 2020). It uses as its main sampling algorithm the affine-invariant ensemble method of Foreman-Mackey et al. (2013) and contains a novel and robust maximiser with reliable convergence towards the global maximum of the posterior.

4.1. ΛCDM

Marginalised posterior distributions are shown in Fig. 1. The corresponding means and 68% confidence intervals are given in Table 1, while Table 2 shows the gain in precision relative to the

[1] www.class-code.net
[2] www.hiclass-code.net
[3] https://github.com/s-ilic/ECLAIR

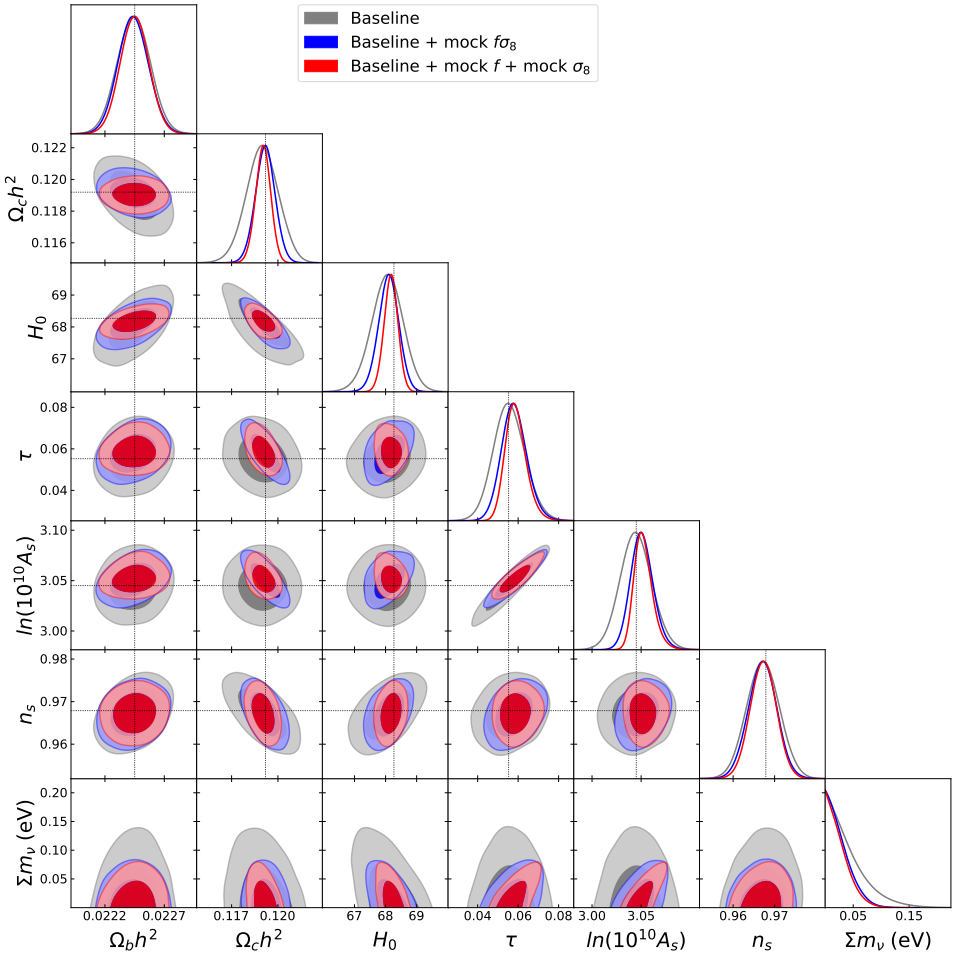

Fig. 1. One-dimensional and two-dimensional marginalised posterior distributions for ΛCDM parameters derived from the baseline only (grey), baseline with mock on $f\sigma_8$ (blue), and baseline with mocks on f and σ_8 (red). The dotted lines indicate the parameter values for the fiducial model (corresponding to the baseline best fit) used when generating mocks.

Table 1. Mean and 68% confidence interval for ΛCDM parameters.

	$f\sigma_8$	$f+\sigma_8$
$\Omega_b h^2$	$0.02244^{0.00013}_{-0.00013}$	$0.02245^{0.00012}_{-0.00012}$
$\Omega_c h^2$	$0.11918^{0.00062}_{-0.00063}$	$0.11904^{0.00048}_{-0.00048}$
H_0	$68.10^{0.32}_{-0.32}$	$68.17^{0.22}_{-0.22}$
τ	$0.0581^{0.0058}_{-0.0066}$	$0.0589^{0.0044}_{-0.0056}$
$\ln(10^{10}A_s)$	$3.0509^{0.0106}_{-0.0121}$	$3.0524^{0.0075}_{-0.0104}$
n_s	$0.9671^{0.0034}_{-0.0034}$	$0.9673^{0.0031}_{-0.0031}$
Σm_ν	$0.0263^{0.0062}_{-0.0263}$	$0.0248^{0.0058}_{-0.0248}$

Notes. The constraints are obtained by combining the baseline with the $f\sigma_8$ mock (middle column) and f and σ_8 mocks (right column).

Table 2. Precision ratios for ΛCDM parameters.

	Baseline $+ f\sigma_8$ /baseline	Baseline $+ f + \sigma_8$ /baseline	Baseline $+ f + \sigma_8$ /baseline + $f\sigma_8$
$\Omega_b h^2$	1.08	1.15	1.06
$\Omega_c h^2$	1.66	2.16	1.30
H_0	1.55	2.26	1.46
τ	1.25	1.54	1.22
$\ln(10^{10}A_s)$	1.40	1.77	1.26
n_s	1.16	1.27	1.09
Σm_ν	1.48	1.57	1.13

Notes. Section 4.1 gives details.

baseline (first two columns) and for the separated growth measurements $f+\sigma_8$ relative to the standard $f\sigma_8$ measurements (last column). We define the precision as the inverse width of the 68% marginalised confidence interval rather than using relative errors, since the latter can become misleading when the mean values are close to zero (e.g., in the case of Σm_ν). In addition, comparing relative errors would also be biased when the mean values shift, as happens for the Horndeski models (see below).

Next-generation surveys are forecast to deliver improved constraints from high-precision RSD $f\sigma_8$ data (see e.g. Amendola et al. 2018; Bacon et al. 2020). The triangle plots and the tables confirm this. Table 2 (first column) shows that the gain in precision ranges from ∼10% for $\Omega_b h^2$ up to more than ∼50% for $\Omega_c h^2$, H_0 and Σm_ν, when considering the addition of the mock data on $f\sigma_8$, with 1% relative error combined to current cosmological data sets.

As expected the constraints improve further with the split mock data on f and σ_8, each with a 1% relative error. This combination performs from 6% to almost 50% better. In particular, the precision on $\Omega_c h^2$ and H_0 is more than doubled relative to the baseline data alone.

The improvement obtained from the split f and σ_8 data over $f\sigma_8$ (as quantified by the third column of Table 2) does not lead to an equal increase in precision on all the parameters that were

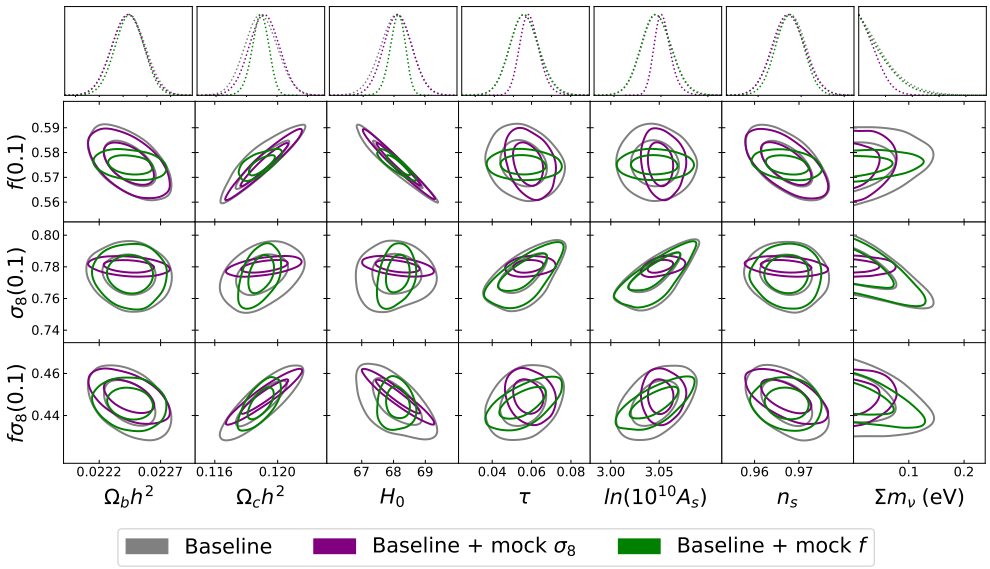

Fig. 2. One-dimensional marginalised posterior distributions (top row) for ΛCDM parameters, from baseline only (grey), baseline + mock on f (green), and baseline + mock on σ_8 (purple). Rows below show 2D posteriors of cosmological parameters against derived parameters f, σ_8, and $f\sigma_8$ at $z = 0.1$.

already well constrained with $f\sigma_8$ RSD data. As an example, we can compare Σm_ν and H_0. Adding $f\sigma_8$ data yields almost a 50% gain on Σm_ν, while the split $f + \sigma_8$ data further increases the precision by 13%. By contrast, H_0 precision first increases by 55% followed by another 46% with the splitting.

The growth probes f, σ_8, and $f\sigma_8$ have different sensitivities to each cosmological parameter, which explains the range of changes in precision. One way to examine those sensitivities is to start with the baseline-only constraints. Figure 2 shows the posterior distributions of f, σ_8, and $f\sigma_8$ at redshift $z = 0.1$ as derived parameters versus the cosmological parameters[4]. Each posterior thus illustrates how a change in a given cosmological parameter impacts the values of the derived growth quantities, taking into account (i.e. marginalising over) the remaining cosmological parameters and how their values need to change to keep a decent fit to the data.

On the other hand, adding constraints on the growth quantities amounts to convolving their posteriors with a Gaussian distribution (with a width equal to 1% of the central value). This in turn may reduce the width of the posterior on cosmological parameters, depending on the amount of correlation between the two. It is thus expected that cosmological parameters that are highly correlated (i.e. thin tilted ellipses) with a given growth quantity in the baseline case, will show the best improvements after including measurements of that growth quantity.

From Fig. 2 we find that Ω_b, Ω_c, H_0, and n_s are better constrained by adding the f mock (green) to the baseline, while τ, A_s, and Σm_ν are better constrained by adding the σ_8 mock (purple). This may appear counter to the common expectation that σ_8 is more sensitive to parameters affecting the power spectrum amplitude, while f is more sensitive to parameters affecting its shape. It is the correlations induced by the baseline constraints that are the decisive factor.

Let us consider an illustrative example from Fig. 2: the 2D posterior of $\{f(0.1), H_0\}$ exhibits a high correlation (thin tilted ellipse), while that of $\{\sigma_8(0.1), H_0\}$ is relatively irregular and close to an uncorrelated case. As a result, the addition of the f mock improves the H_0 constraint significantly more relative to the baseline (see the 1D posterior of H_0 in the top row of Fig. 2).

These correlations can even lead to improved constraints on parameters that f and σ_8 should not depend on. An example is the tight constraint on the reionisation parameter τ produced by the mock on σ_8, which originates in the tight constraint on A_s from σ_8, combined with the underlying high correlation between A_s and τ, as shown in Fig. 1. A tight constraint on τ is obtained even though it does not play a role in the value of σ_8.

4.2. Horndeski

The Horndeski parameter space is extended to include modifications in the background (w_0, w_a) and in the perturbations $(\alpha_M, \alpha_K, \alpha_B)$. Marginalised posterior distributions with the baseline and mock data sets are displayed in Fig. 3, with the corresponding means and 68% confidence intervals in Table 3. We observe that the maximum of the posterior distribution for the extension parameters shifts significantly towards the best-fit model (dotted lines), while the contours assume a much more regular, ellipsoidal shape compared to the baseline case. This is expected in a transition from a regime where priors still play a significant role (as discussed at the end of Sect. 3), to a situation where data dominate the posterior. Interestingly, these results also show that if the true underlying cosmology is indeed close to the Horndeski best-fit fiducial, then growth data with 1% relative precision (over the redshift range considered) could lead to the detection of this deviation from ΛCDM with strong significance (more than 5σ).

Table 4 shows the gain in precision relative to the baseline (first two columns) and for the separated growth measurements $f + \sigma_8$ relative to the standard $f\sigma_8$ measurements (last column). As pointed out earlier, the kineticity coupling α_K is not constrained by the data and is therefore not included in the figure and tables, but a_K is included as a free parameter in the analysis. The accuracy that was gained on the cosmological parameters in ΛCDM is largely lost. Adding the mock on $f\sigma_8$ only delivers a precision gain of up to ∼20% (see Table 4). This can

[4] We find the orientations of these posteriors (i.e. correlation factors between parameters) to change very little with redshift. Therefore we consider only $z = 0.1$ for illustration, but our discussion applies to the other z.

Table 3. Mean and 68% confidence interval for Horndeski parameters.

	$f\sigma_8$	$f+\sigma_8$
$\Omega_b h^2$	$0.02259^{0.00015}_{-0.00014}$	$0.02258^{0.00015}_{-0.00015}$
$\Omega_c h^2$	$0.11801^{0.00122}_{-0.00122}$	$0.11819^{0.00122}_{-0.00122}$
H_0	$68.44^{0.96}_{-0.96}$	$68.69^{0.85}_{-0.85}$
τ	$0.0508^{0.0075}_{-0.0075}$	$0.0526^{0.0070}_{-0.0068}$
$\ln(10^{10}A_s)$	$3.0324^{0.0157}_{-0.0155}$	$3.0366^{0.0140}_{-0.0136}$
n_s	$0.9704^{0.0042}_{-0.0042}$	$0.9702^{0.0042}_{-0.0042}$
Σm_ν	$0.0953^{0.0261}_{-0.0953}$	$0.0742^{0.0206}_{-0.0742}$
w_0	$-0.9636^{0.0862}_{-0.0797}$	$-0.9770^{0.0813}_{-0.0814}$
w_a	$-0.1901^{0.2632}_{-0.2636}$	$-0.1543^{0.2984}_{-0.2494}$
a_B	$1.9493^{0.1801}_{-0.2058}$	$1.9262^{0.1791}_{-0.2003}$
a_M	$3.3473^{0.4411}_{-0.5943}$	$3.0485^{0.2630}_{-0.3799}$

Notes. The constraints are obtained by combining the baseline with the $f\sigma_8$ mock (middle column) and f and σ_8 mocks (right column).

Table 4. Precision ratios for Horndeski parameters.

	Baseline $+ f\sigma_8$ /baseline	Baseline $+ f + \sigma_8$ /baseline	Baseline $+ f + \sigma_8$ /baseline + $f\sigma_8$
$\Omega_b h^2$	1.11	1.10	0.99
$\Omega_c h^2$	1.20	1.20	1.00
H_0	1.19	1.35	1.12
τ	0.96	1.04	1.05
$\ln(10^{10}A_s)$	0.98	1.11	1.13
n_s	1.10	1.10	1.00
Σm_ν	1.49	1.91	1.65
w_0	1.29	1.32	1.01
w_a	1.65	1.59	1.18
a_B	2.83	2.87	1.03
a_M	3.30	5.32	1.77

Notes. Section 4.2 gives details.

be attributed to the addition of new, poorly constrained degrees of freedom, which naturally leads to larger errors on all the original parameters via correlations, as both sets may have similar and degenerate effects on the growth of structure. For example, Fig. 3 shows how a_M and a_B are relatively degenerate with other parameters when using the baseline data only.

However, there is significant improvement for the extension parameters: adding future $f\sigma_8$ data yields a 230% improvement for the running of the effective Planck mass α_M and a remarkable ~50% gain for Σm_ν. Even though $f\sigma_8$ is a probe of the perturbations, adding its mock to the baseline achieves a surprising ~30% and ~60% gain in precision for w_0 and w_a respectively.

The additional gain from disentangling f and σ_8 measurements is also subject to the effects of opening up the parameter space. The standard parameters see little improvement (<15%) over the $f\sigma_8$ case. By contrast, w_a, Σm_ν, and α_M precisions jump by a further ~20%, ~65%, and ~80% respectively.

The underlying reason why growth data provide such an enhancement in precision for the Horndeski parameters is rooted in the modification of gravitational dynamics (e.g. the Poisson equation) by α_I. As discussed in Perenon et al. (2019), these modifications produce two opposing contributions:
* a fifth force, enhancing growth;
* a higher effective Planck mass, suppressing growth.

The effective Planck mass is controlled solely by α_M for the models we consider. As a result, growth data strongly constrains a_M and also a_B. Table 4 shows that the splitting of $f\sigma_8$ into f and σ_8 is very effective to further constrain a_M, thereby disentangling the fifth force and effective Planck mass contributions. This feature was seen even with current split data in Perenon et al. (2019).

The modified background parameters w_0 and w_a also contribute to the growth of structure through Hubble friction. Their effects on growth are therefore degenerate with those of α_I. We see in Fig. 4 that w_0, w_a, a_B, and a_M display some degeneracies in their 2D marginalised posteriors.

Following the arguments for ΛCDM, we can understand the separate improvements from f and σ_8 by analysing their posterior distributions versus cosmological parameters, shown in Fig. 4. We note that the stability requirements for the Horndeski models induce highly non-Gaussian posterior distributions, which makes the analysis more subtle. Figure 4 shows that f correlates more strongly with a_B and a_M than σ_8, so that adding f measurements results in a larger increase in precision for these parameters. Since these two parameters control the strength of the fifth force, this could be expected, given that σ_8 is an integrated function of f, which tends to wash out the effects of the fifth force. The fifth force is an effect occurring at low redshifts as opposed to the effect of Hubble friction or neutrinos. A chain of correlations – seen in the baseline constraints – shows that σ_8 brings a larger gain in precision for w_0, w_a, and Σm_ν. This signals therefore a higher sensitivity of σ_8 to modifications of gravity spanning longer periods.

It is in fact expected that the effect of neutrinos is partially degenerate with that of modified gravity (see e.g. Wright et al. 2019; Ballardini et al. 2020). Massive neutrinos suppress the growth of structure on small scales, which can either oppose or reinforce modified gravity, depending on whether the fifth force or the Planck mass running is favoured. Horndeski models compatible with current RSD $f\sigma_8$ constraints produce a suppression of growth at late times (Perenon et al. 2019).

The baseline constraints in Fig. 3 show that the 2D posteriors of Σm_ν with a_B and a_M have a fairly irregular shape, while those with w_0 and w_a are more correlated. More surprisingly, as noted above, Σm_ν has almost a 50% gain with the addition of the $f\sigma_8$ mock data, as in the case of ΛCDM. The splitting improves constraints by a further 70% as opposed to 7% in ΛCDM. It is therefore clear that these growth mocks break the neutrino-modified gravity degeneracy by efficiently constraining Σm_ν and the extension parameters. Figure 4 tells us that this is rooted in the correlation of Σm_ν with σ_8 in the baseline.

On the other hand, we also see that all the intricate degeneracies between the extension parameters and standard model parameters render the baseline constraints for the latter much less correlated than in the case of ΛCDM. This explains why the improvements from the splitting are not as great in the case of Horndeski for the other standard parameters. We note that when the background evolution is fixed to that of ΛCDM, Σm_ν displays a correlation with α_B (Bellomo et al. 2017). Here, the freedom that arises from varying w_0 and w_a lessens that correlation.

4.3. Extending the redshift range

Having understood better the influence of each mock data set on the constraints, we now assess the effect of extending the

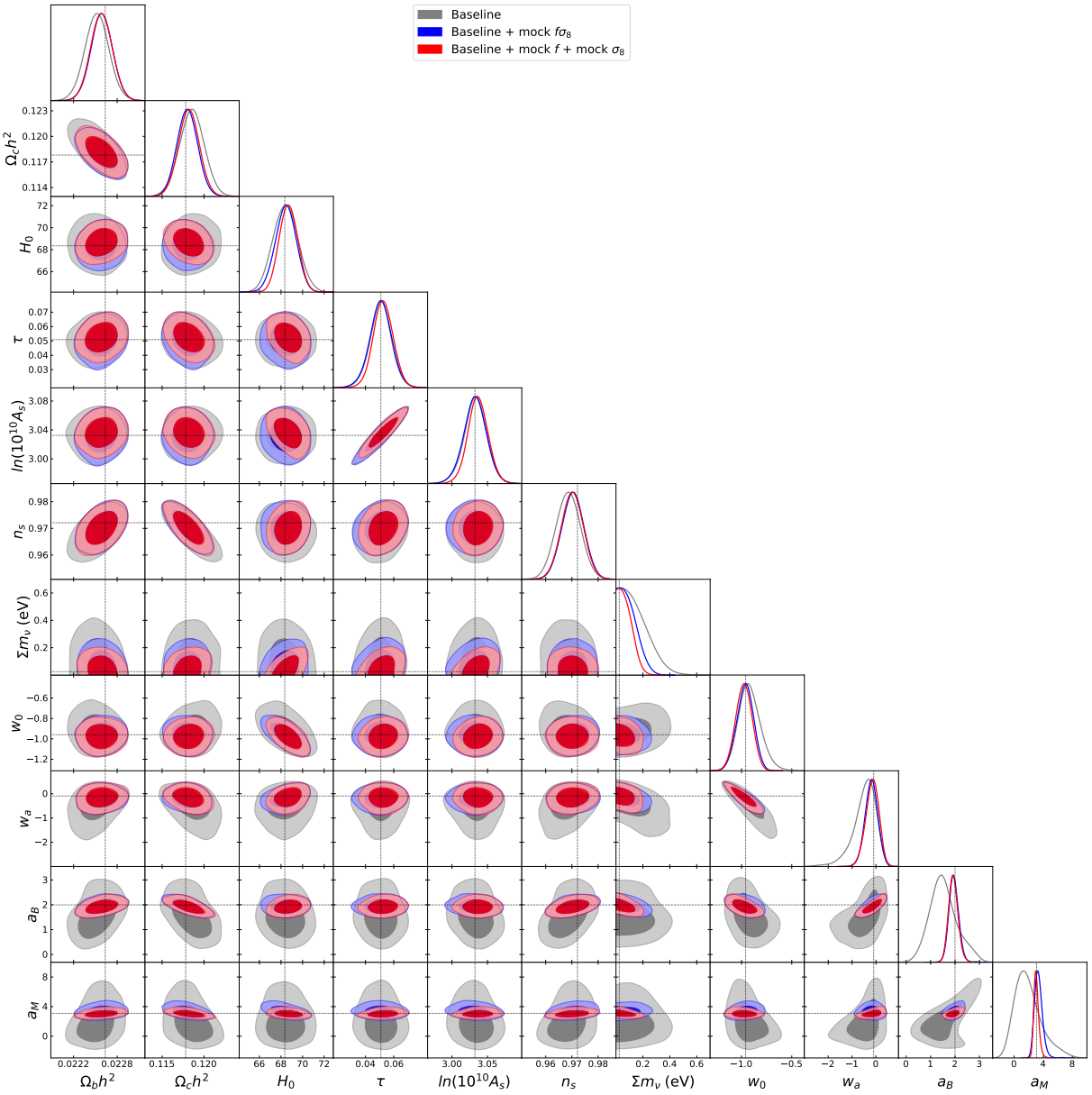

Fig. 3. One-dimensional and two-dimensional marginalised posterior distributions for Horndeski parameters derived from the baseline only (grey), baseline with mock on $f\sigma_8$ (blue), and baseline with mocks on f and σ_8 (red). The dotted lines indicate the parameter values for the fiducial model (corresponding to the baseline best fit) used when generating mocks.

redshift coverage of the mocks. More specifically, we examine the respective merits of adding $f\sigma_8$ or $f + \sigma_8$ measurements, when extending the maximum redshift of each mock. Table 5 shows that the combined data $f\sigma_8$ with $z_{\rm max} = 2$ (first column) performs no better than $f + \sigma_8$ data with half the redshift range ($z_{\rm max} = 1$, see Tables 1 and 3). We find that extending the redshift range further improves the precision up to 30% with respect to $z_{\rm max} = 1$ in the case of the combined mock $f\sigma_8$ for ΛCDM and Horndeski models, and respectively 20% and 15% in the case of f and σ_8 mocks.

5. Conclusion

Upcoming galaxy surveys such as Euclid (Amendola et al. 2018) and Square Kilometre Array (SKA; Bacon et al. 2020) with their unprecedented precision is a call to sharpen our tools for constraining gravity. One cosmological probe well suited for that task is the growth of structure. This toolbox is further complemented by the releases of measurements on f and σ_8 (de la Torre et al. 2017; Shi et al. 2018; Jullo et al. 2019; Gil-Marín et al. 2017).

In this paper, we considered the performance that a future nominal galaxy sample can deliver with a ∼1% relative error on f and σ_8 separately and on the combination $f\sigma_8$. We compared the constraints from the separated data with those from the combination data. We assumed ten measurements per growth quantity equally spread over the redshift range $z = 0.1, 0.2, \ldots, 1.0$. For the case of ΛCDM, the improvements in precision range over ∼5–50%. For modified gravity described by Horndeski models, the improvements on these standard model parameters reduce to ∼0–15%.

However, the splitting of f and σ_8 stands out as very effective in breaking the neutrino – modified gravity degeneracy, with the sum of neutrino masses enjoying an improvement of 65% over

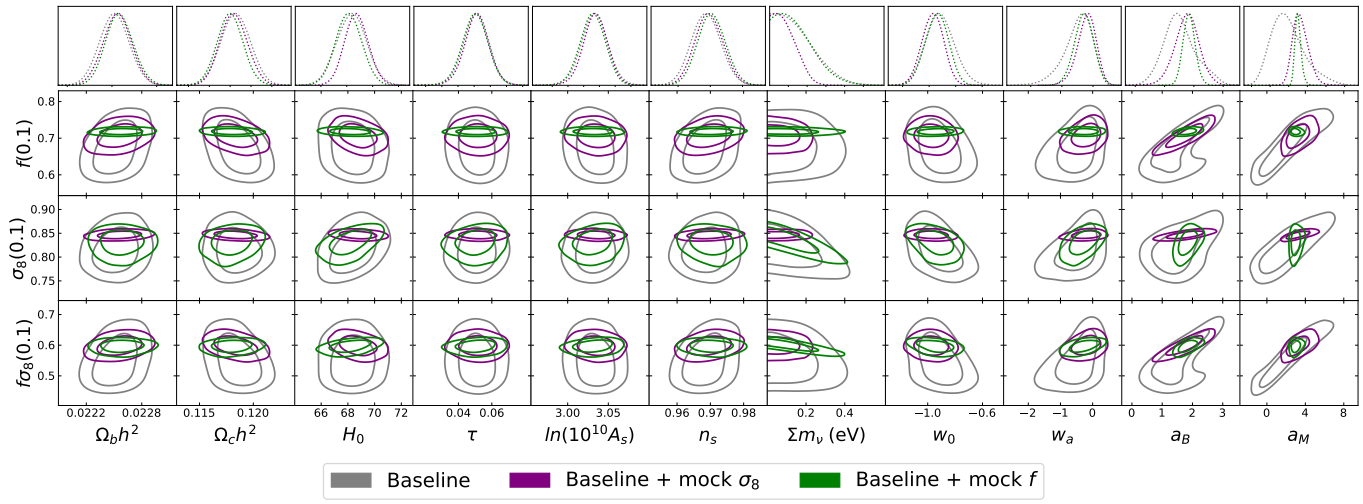

Fig. 4. One-dimensional marginalised posterior distributions (*top row*) for Horndeski parameters, from baseline only (grey), baseline + mock on f (green), and baseline + mock on σ_8 (purple). Rows below show 2D posteriors of cosmological parameters against derived parameters f, σ_8, and $f\sigma_8$ computed at $z = 0.1$.

Table 5. Mean and 68% confidence interval for ΛCDM (*top*) and Horndeski (*bottom*) parameters with the redshift of the mocks extended to $z = 0.1, 0.2, \ldots, 2.0$.

	$f\sigma_8$ ($z_{\max} = 2$)	$f + \sigma_8$ ($z_{\max} = 2$)
$\Omega_b h^2$	$0.02245^{0.00012}_{-0.00012}$	$0.02244^{0.00012}_{-0.00012}$
$\Omega_c h^2$	$0.11910^{0.00055}_{-0.00054}$	$0.11907^{0.00046}_{-0.00046}$
H_0	$68.17^{0.25}_{-0.25}$	$68.17^{0.21}_{-0.21}$
τ	$0.0588^{0.0045}_{-0.0056}$	$0.0587^{0.0038}_{-0.0048}$
$\ln(10^{10}A_s)$	$3.0524^{0.0075}_{-0.0102}$	$3.0521^{0.0062}_{-0.0089}$
n_s	$0.9673^{0.0032}_{-0.0033}$	$0.9673^{0.0031}_{-0.0031}$
Σm_ν	$0.0234^{0.0055}_{-0.0234}$	$0.0234^{0.0055}_{-0.0234}$
$\Omega_b h^2$	$0.02259^{0.00015}_{-0.00015}$	$0.02258^{0.00015}_{-0.00015}$
$\Omega_c h^2$	$0.11813^{0.00123}_{-0.00123}$	$0.11824^{0.00117}_{-0.00117}$
H_0	$68.60^{0.88}_{-0.88}$	$68.63^{0.82}_{-0.81}$
τ	$0.0523^{0.0071}_{-0.0072}$	$0.0524^{0.0071}_{-0.0071}$
$\ln(10^{10}A_s)$	$3.0357^{0.0144}_{-0.0143}$	$3.0365^{0.0141}_{-0.0143}$
n_s	$0.9702^{0.0042}_{-0.0042}$	$0.9701^{0.0041}_{-0.0041}$
Σm_ν	$0.0656^{0.0181}_{-0.0656}$	$0.0693^{0.0185}_{-0.0693}$
w_0	$-0.9761^{0.0840}_{-0.0850}$	$-0.9764^{0.0705}_{-0.0710}$
w_a	$-0.1328^{0.2831}_{-0.2542}$	$-0.1452^{0.2666}_{-0.2167}$
a_B	$1.9494^{0.1710}_{-0.1939}$	$1.9266^{0.1594}_{-0.1857}$
a_M	$3.1274^{0.3142}_{-0.4618}$	$3.0552^{0.2409}_{-0.3672}$

Notes. The constraints are obtained by combining the baseline with the $f\sigma_8$ mock (middle column) and f and σ_8 mocks (right column).

the case with only $f\sigma_8$ data. We also find a significant increase in the precision on the background and perturbation Horndeski parameters, with an additional gain of ∼20% for the varying effective DE equation of state parameter w_a and ∼80% for the evolution of the effective Planck mass a_M. Extending the redshift of the mocks up to $z_{\max} = 2$ shows that the constraints provided by the combined $f\sigma_8$ data are already matched by the split data f and σ_8 with $z_{\max} = 1$.

Our results highlight that growth data, whether split or combined and with 1% relative error could lead to the detection of deviations from ΛCDM with strong significance (more than 5σ), should the underlying cosmology be close to the current Horndeski best-fit fiducial. The splitting of growth data on $f\sigma_8$ into data on f and σ_8 with galaxy-galaxy lensing (de la Torre et al. 2017; Shi et al. 2018; Jullo et al. 2019) or by combinations with the bispectrum (Gil-Marín et al. 2017) emerges clearly from this work as both a powerful complementary probe for the standard model and a stringent probe to detect departures from it. The latter could prove crucial in the era of future surveys, given the current tensions within the standard model and the emergence of alternative models of gravity favoured by Bayesian evidence (Peirone et al. 2019; Solà Peracaula et al. 2019).

Acknowledgements. We are grateful to Julien Bel for helpful exchanges and feedback on the draft. We thank Matteo Martinelli for useful discussions. The authors acknowledge the Sciama High Performance Compute Cluster, which is supported by the ICG at the University of Portsmouth, and the CHPC the Centre for High Performance Computing (CHPC), South Africa, for providing computational resources for this research project. LP and RM are supported by the South African Radio Astronomy Observatory (SARAO) and the National Research Foundation (Grant No. 75415). RM is also supported by the UK STFC Consolidated Grant ST/N000668/1. SI was supported by the European Structural and Investment Fund and the Czech Ministry of Education, Youth and Sports (Project CoGraDS – CZ.02.1.01/0.0/0.0/15_003/0000437). AdlCD acknowledges financial support from NRF Grants No.120390, Reference: BSFP190416431035 and No.120396, Reference: CSRP190405427545, Project No. FPA2014-53375-C2-1-P from the Spanish Ministry of Economy and Science, Project No. FIS2016-78859-P from the European Regional Development Fund and Spanish Research Agency (AEI), and support from Projects Nos. CA15117 and CA16104 from COST Actions EU Framework Programme Horizon 2020.

References

Abazajian, K. N., Adshead, P., Ahmed, Z., et al. 2016, ArXiv e-prints [arXiv:1610.02743]
Abbott, B., Abbott, R., Abbott, T. D., et al. (LIGO Scientific Collaboration and Virgo Collaboration) 2017a, Phys. Rev. Lett., 119, 161101
Abbott, B., Abbott, R., Abbott, T. D., et al. 2017b, ApJ, 848, L13
Alonso, D., Bellini, E., Ferreira, P. G., & Zumalacarregui, M. 2017, Phys. Rev. D, 95, 063502
Amendola, L., Appleby, S., Avgoustidis, A., et al. 2018, Liv. Rev. Rel., 21, 2
Anderson, L., Aubourg, É., Bailey, S., et al. 2014, MNRAS, 441, 24
Bacon, D. J., Battye, R. A., Bull, P., et al. 2020, PASA, 37, e007

Ballardini, M., Sapone, D., Umiltà, C., Finelli, F., & Paoletti, D. 2019, JCAP, 05, 049
Ballardini, M., Braglia, M., Finelli, F., et al. 2020, JCAP, 2020, 008
Bellini, E., & Sawicki, I. 2014, JCAP, 1407, 050
Bellini, E., Cuesta, A. J., Jimenez, R., & Verde, L. 2016, JCAP, 1602, 053; erratum: JCAP1606, no.06, E01(2016)
Bellini, E., Sawicki, I., & Zumalacarregui, M. 2020, J. Cosmol. Astropart. Phys., 2, 008
Bellomo, N., Bellini, E., Hu, B., et al. 2017, JCAP, 1702, 043
Betoule, M., Kessler, R., Guy, J., et al. 2014, A&A, 568, A22
Beutler, F., Blake, C., Colless, M., et al. 2011, MNRAS, 416, 3017
Blas, D., Lesgourgues, J., & Tram, T. 2011, JCAP, 1107, 034
Bloomfield, J. K., Flanagan, E. A., Park, M., & Watson, S. 2013, JCAP, 1308, 010
Chevallier, M., & Polarski, D. 2001, Int. J. Mod. Phys. D, 10, 213
de la Torre, S., Guzzo, L., Peacock, J. A., et al. 2017, A&A, 608, A44
Foreman-Mackey, D., Hogg, D. W., Lang, D., & Goodman, J. 2013, PASP, 125, 306
Frusciante, N., & Perenon, L. 2020, Phys. Rept., 857, 1
Frusciante, N., Peirone, S., Casas, S., & Lima, N. A. 2019, Phys. Rev. D, 99, 063538
Gil-Marín, H., Percival, W. J., Verde, L., et al. 2017, MNRAS, 465, 1757
Gleyzes, J., Langlois, D., Mancarella, M., & Vernizzi, F. 2016, JCAP, 02, 056
Gubitosi, G., Piazza, F., & Vernizzi, F. 2013, JCAP, 1302, 032
Horndeski, G. W. 1974, Int. J. Theor. Phys., 10, 363
Ilić, S., Kopp, M., Skordis, C., & Thomas, D. B. 2020, A&A, submitted [arXiv:2004.09572]
Jullo, E., de la Torre, S., Cousinou, M.-C., et al. 2019, A&A, 627, A137
Kreisch, C. D., & Komatsu, E. 2018, JCAP, 1812, 030
Leung, J. S.-Y., & Huang, Z. 2017, Int. J. Mod. Phys. D, 26, 1750070
Linder, E. V. 2003, Phys. Rev. Lett., 90, 091301
Peirone, S., Benevento, G., Frusciante, N., & Tsujikawa, S. 2019, Phys. Rev. D, 100, 063540
Perenon, L., Bel, J., Maartens, R., & de la Cruz-Dombriz, A. 2019, JCAP, 1906, 020
Piazza, F., Steigerwald, H., & Marinoni, C. 2014, JCAP, 1405, 043
Planck Collaboration V. 2020, A&A, 641, A5
Reischke, R., Spurio Mancini, A., Schafer, B. M., & Merkel, P. M. 2019, MNRAS, 482, 3274
Ross, A. J., Samushia, L., Howlett, C., et al. 2015, MNRAS, 449, 835
Shi, F., Yang, X., Wang, H., et al. 2018, ApJ, 861, 137
Solà Peracaula, J., Gomez-Valent, A., de Cruz Pérez, J., & Moreno-Pulido, C. 2019, ApJ, 886, L6
Spurio Mancini, A., Reischke, R., Pettorino, V., Schafer, V., & Zumalacárregui, M. 2018, MNRAS, 480, 3725
Wright, B. S., Koyama, K., Winther, H. A., & Zhao, G.-B. 2019, JCAP, 06, 040
Zumalacarregui, M., Bellini, E., Sawicki, I., Lesgourgues, J., & Ferreira, P. G. 2017, JCAP, 1708, 019